Arabian Journal for Science and Engineering
https://doi.org/10.1007/s13369-018-3391-z

RESEARCH ARTICLE - MECHANICAL ENGINEERING

Discrete-Phase Modelling of an Asymmetric Stenosis Artery Under Different Womersley Numbers

B. Prashantha[1] · **S. Anish**[1]

Received: 11 July 2017 / Accepted: 3 June 2018

Abstract
Understanding the hemodynamics in the post-stenotic region of an asymmetric stenosis is of paramount importance in the study of atherosclerosis progression. Numerically, the analysis becomes more complex when a discrete phase is added to the continuous phase in order to understand the behaviour of atherogenic particles in a pulsatile flow environment. In the present study, discrete-phase modelling (DPM) of an asymmetric and symmetric stenosed artery models has been carried out at different Womersley numbers. The objective is to understand the correlation between the discrete-phase (atherogenic) particle behaviour with the characteristics of continuous phase (blood) under varying pulse frequencies. Continuous phase is modelled by time-averaged Navier–Stokes equations and solved by means of pressure implicit splitting of operators algorithm. DPM has been carried out with one-way coupling. The transport equations are solved in the Eulerian frame of reference, and the discrete phase is simulated in Lagrangian frame of reference. The study brings out the importance of helicity in the atherosclerosis progression. Result shows that the asymmetric stenosis model exhibits less helical flow structure and the vortical structures are not getting transported to the downstream. Consequently, the average particle residence time (PRT) of the atherogenic particles is one order higher than the symmetric stenosis model. Low PRT leads to enhanced mass transport in the arterial flow and triggers further occlusion/plaque build-up at the post-stenotic region. The extent of asymmetry in a diseased artery may be considered as a useful parameter in understanding the rate of progression of atherosclerosis.

Keywords Stenosis · Womersley number · Discrete-phase modelling · Helicity

1 Introduction

Atherosclerosis is a common dangerous disease and causes death in many countries because of pulsatile blood behaviour and complex geometries in the human arterial system [1]. Several autopsy studies have been demonstrated that 70–80% of cardiovascular diseases occurs at complex geometries [1–3]. Deposition of lipids in the arterial passage is not uniform, and hence, stenotic plaques acquire a complex structure inside the lumen. Due to nature of arterial wall geometry and pulsatile flow nature, deposition concentration will occur more at one side of an arterial wall, resulting in an asymmetric occlusion. Considerable numerical investigations have been carried out till date, in realistic and idealized symmetric stenosis model, to understand the blood flow behaviour (hemodynamics) in severe stenosed arteries. However, limited studies are available correlating the behaviour of atherogenic particles with the hemodynamic characteristics in a severe stenosed artery. Such a study becomes even more complex (and realistic), when the flow is pulsatile and the stenosis is asymmetric.

Majority of the earlier works were carried out using symmetric stenosis, and very few works were reported on the pulsatile flow through asymmetric stenosis. A relevant addition in that real-life stenosis is more likely to be eccentric rather than axisymmetric. Stenosis eccentricity causes the jet to deflect towards the side of the eccentricity. A notable work was carried out by Varghese et al. [4] and Dvinsky and Ojha [5], wherein a geometric perturbation was given in the form of a stenosis eccentricity. Varghese et al. [4] more focused on the periodic transition to turbulence and subsequent re-laminarization of post-stenotic flow. Jabir and Lal [6] attempt to solve the flow through a stenosis having asymmetric elliptic cross section with an eccentricity, which

✉ S. Anish
anish@nitk.edu.in

[1] Department of Mechanical Engineering, Centre for Biomedical Engineering, National Institute of Technology, Karnataka, India

Published online: 13 June 2018

is a logical extension of the model towards the actual physiological situation. They established that the flow is fully turbulent at the post-stenotic region of an eccentric stenosis. A swirling flow can suppress further development of stenosis by enhancing the transport and mixing of the blood flow. This was shown by Ha et al. [7] using a time-resolved particle image velocimetry (PIV) technique. They observed the generation of several near wall vortices in a swirling flow. The swirling flow may induce more helicity to the post-stenotic region. The helical blood flow may lessen the burden of arteries and protect the arteries from the pathology of atherosclerosis, thrombosis, and intimal hyperplasia [2]. Though the presence of helical flow has pattern observed at several sites of the vascular system, its presence and importance at the post-stenotic region of an asymmetric stenosis are not clearly understood.

Surface topology of the arteries is an important aspect in the numerical study of hemodynamics. Simulations on patient-specific geometries were carried out by Basavaraja et al. [8], and the role of wall shear stress (WSS), oscillatory shear index (OSI) and vorticity, on the generation and progression of atherosclerosis is identified. However, replicating patient anatomy does not necessarily lead to more relevant results in terms of understanding specific characteristics of the hemodynamics [9]. To reduce uncertainties in the simulations with specific patient geometry and also for the easiness in parametric variation studies, an idealized model is more suitable [10]. The simplification to an idealized model is well accepted in large arteries (Aorta, Carotid etc.,) because the non-Newtonian nature of the blood and arterial wall compliance was found to play lesser role in the atherogeneses of these arteries [11–13]. For a given artery and a given inlet velocity profile, the hemodynamics greatly depends on the pulse frequency. The Womersley number ($\alpha = R\sqrt{\omega/\nu}$) is a useful non-dimensional number which connects the arterial size to the pulse frequency. In the above expression 'R' is the artery radius, 'ω' is the angular frequency, and 'ν' is the kinematic viscosity of the blood. For a given artery radius, the changes in Womersley number directly signify the variations in the pulse frequency, which in turn depends on the physiological condition of the body. Womersley number for the pulsatile flow will be different in the human arterial system and usually varies from 1 to 12. The numerical simulations carried out by Buchanan et al. [14] and Banerjee et al. [15] revealed an increased flow disturbances with pulse frequency. Hence, the effect of pulse frequency variation on hemodynamics is extremely important and not much studies have been undertaken on this aspect particularly in a diseased artery flow.

The objective of the present numerical investigation is to understand the correlation between behaviour of the discrete-phase atherogenic particles with the characteristics of continuous phase in a more realistic asymmetrically stenosed artery. Particular emphasis is given to understand the effect of variations in the pulse frequencies of blood flow on the particle trajectories and the blood flow dynamics. The novelty of this study lies in the use of discrete-phase modelling in a pulsatile flow environment. Comparative studies are carried out using a symmetric and asymmetric stenosed channel under three different Womersley numbers, and the atherogenic particles behaviour is noted down in terms of residence time, velocity and particle trajectory. As different pulse rates correspond to different physiological conditions of the artery, the present investigation attempts to identify the hemodynamic scenarios which are more critical to atherosclerotic progression.

2 Model Description

The topology of arterial lumen is highly irregular and unique for each subject. Hence, the simulations with patient-specific geometry create difficulties in identifying and separate out the effect of any single parameter on the flow behaviour. The present investigation focuses on understanding the effect of two important parameters on the hemodynamics as well as the particle behaviour. These are pulse frequency of the flow and the eccentricity of the stenosis. First one is a dynamic characteristic of the flow, and the second one is geometry related.

The geometry of the idealized artery model is scaled up with dynamic similarity point of view. Along with the asymmetrically stenosed model, one symmetric model is also used for this study. The symmetric model acts as a basis for comparison for the asymmetric model. The dimensions of symmetric model have been taken from the model used by Ahmed and Giddens [16] for their experimental analysis. The diameter (D) at the non-stenosed portion is taken as two inch. Though this value is far beyond the physiological range, this diameter is considered to compare with the experimental results of Ahmed and Giddens [16]. Similar to the experimental set-up, the computational geometry is given an upstream stenotic length of $94D$ (Fig. 1). This makes sure that the flow is fully developed before it reaches the stenosed portion. The post-stenotic region has a length of $36D$, while the stenosis region is having a length of $4D$. The profile in the symmetric stenosis region is varied by using a cosine function [17] and is shown below.

$$
\begin{aligned}
S(x) &= \{(R_0 - R_0 S_0[1 - \cos(2\pi(x - x_1)/(x_2 - x_1))]/2\} \\
x_1 &< x < x_2 \\
x_1 &= -2D \\
x_2 &= 2D \\
S_0 &= (A - a)/A
\end{aligned} \tag{1}
$$

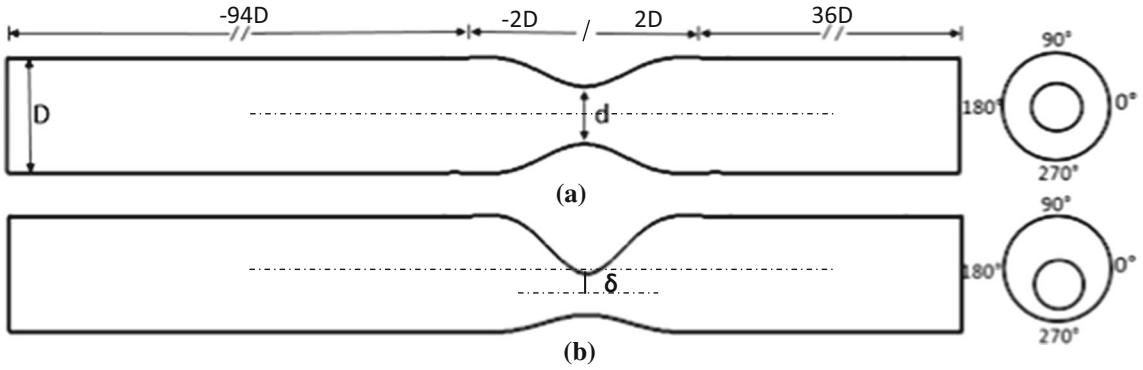

Fig. 1 Schematic representation of idealized stenosed arteries **a** symmetric stenosis, **b** asymmetric stenosis with 15% eccentricity

R is the radius of the straight tube, A is the cross-sectional area of the non-stenosed part, and a is the minimum cross-sectional area at the stenosis.

The asymmetry is generated by providing a 15% eccentricity ($e = \frac{\delta}{D}$) to the stenosis centre in the 90°–270° plane (Fig. 1b). The three-dimensional model has been generated using CATIA, and the grid generation is carried out using ICEMCFD. The degree of stenosis (S_0) was kept as 75% in all the numerical simulations. The boundary wall is assumed to be rigid, and no slip condition is specified [14,15,18–21]. As the wall deformation is planned to consider in the next phase of investigation, the present study focuses only on the discrete-phase modelling of flow through an eccentric channel.

2.1 Mathematical Formulation

The computational domain consists of a continuous phase, with properties similar to blood, and a discrete particular phase with similar physical properties of atherogenic particles like LDL, monocytes [21–23]. Finite volume method (FVM) coupled with discrete-phase modelling (DPM) is used to compute the trajectories of suspended particles in a particular flow environment. While the transport equations are solved in the Eulerian frame of reference, the discrete phase is simulated in Lagrangian frame of reference.

2.2 Continuous-Phase Modelling

Blood is treated as continuum by solving time-averaged Navier–Stokes equation by means of pressure implicit splitting of operators (PISO) algorithm of ANSYS FLUENT. PISO is a pressure-based segregated algorithm. The second-order unwinding scheme is used for momentum equation. The turbulence methodology adopted for this study is the traditional RANS simulation with standard k-omega model which incorporates low Reynolds number effects and shear flow spreading. Turbulence intensity of 7.2% and a length scale of 0.003556 m are used as recommended to fully developed flows by ANSYS FLUENT [24]. The objective of the present work is to understand the effect of pulse frequency on the hemodynamics of a stenosed artery, for which the authors have used a simplified cosine function as an input boundary condition. Such an idealized approach will enable to carry out a more rigorous systematic study, by varying one specific variable at a time while keeping the others constant. Hence, inflow waveform is considered as a cosine wave similar to the one used by Ahmed and Giddens [16] for the in vitro analysis and the velocity profile as a function of time (t) may be expressed as below.

$$V(t) = \left\{ u_{\text{avg}} + \left[(u_{\text{peak}} - u_{\text{avg}}) \times \cos\left(\frac{2\pi t}{T} - 2.53 \right) \right] \right\} \tag{2}$$

where 'u_{avg}' is the average velocity, 'u_{peak}' is the peak velocity, 't' is the time instances in the pulse, and 'T' is the pulse period time. Figure 2 shows the normalized inflow waveform. Four time instances are marked on this waveform corresponding to the accelerating (T_1), peak (T_2), decelerating (T_3) and base velocities (T_4) of the pulse flow. Detailed hemodynamic analysis has been carried out at these four specific time instances. As the present study focuses only on the effect of pulse rate, similar velocity profiles are used for all the cases with varying Womersley numbers.

To achieve similarity to the human non-bifurcating artery, Reynolds number (based on the centreline velocity) in the artery model has to vary between 200 and 1000 [13,16,25]. The time period for one pulse is taken as 20, 14 and 7.7 s, and the corresponding Womersley numbers (α) are 7.5, 9 and 12, respectively. The number of iterations in the inner loop has been set to 30 with a time step size of 0.001 s. The convergence criterion for each time step is governed by a residual criterion of 10^{-7}. Blood is modelled as Newtonian fluid with density and dynamic viscosity as 1000 Kg/m^3 and 0.0036014 Pa s, respectively [16,26–28]. Simulations are run

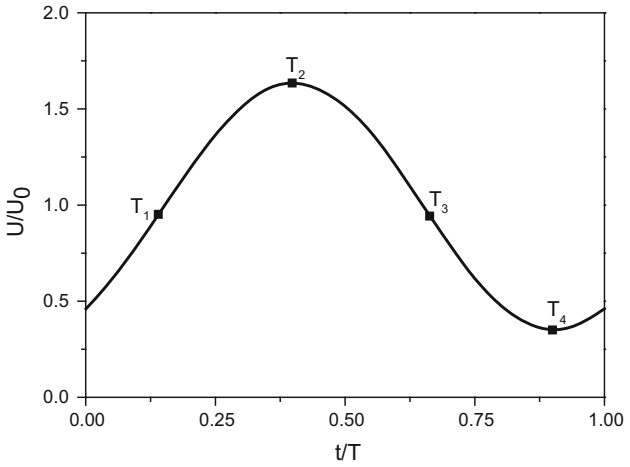

Fig. 2 Inflow velocity profile. T_1, T_2, T_3 and T_4 are the time instances corresponding to the accelerating, peak, decelerating and base velocities used for the analysis

for a sufficient number of pulse cycles until a solution meets the convergence criteria.

2.3 Discrete-Phase Modelling

Discrete-phase modelling has been carried out by tracking a number of particles through the calculated flow field of continuous phase. Particle interaction with the local flow structures plays a significant role; hence, the modelling has been carried out with one-way coupling. The influence of continuous phase on particles behaviour alone is significant, and the continuous phase is not affected by the particles. This assumption is fairly applicable, as the discrete phase had only a volume fraction of 2% in the computational domain. The atherogenic particles are assumed to be spherical with mean diameter of 5 microns. Particles were released from the inlet surface uniformly, and they are accelerated by the resultant force upon interaction with the continuous liquid phase. The particle–wall interaction is assumed to be an elastic collision and modelled accordingly. Interaction between the wall and particles is described with coefficient of restitution (e_n), and it can be expressed as

$$e_n = \frac{v_{2,n}}{v_{1,n}} \tag{3}$$

where v_n is the particle velocity normal to the wall and subscripts 1 and 2 refer to before and after the collision. A normal or tangential coefficient of restitution equal to one implies that the particle retains all of its normal or tangential momentum after the rebound (an elastic collision law). Elastic collision sometimes will be less than one also; it depends upon the property of the particles. A normal or tangential coefficient of restitution equal to zero implies that the particle retains none of its normal or tangential momentum after the rebound [24]. In case of a moving wall, the coefficients need to consider the velocity of the wall.

The trajectory of a discrete-phase particle was predicted by integrating the force balance on the particle. In a Lagrangian frame of reference, the particle's inertia with the force can be written as Eq. (5).

$$\frac{dx}{dt} = u_p \tag{4}$$

$$\frac{d\vec{u}_p}{dt} = F_D(\vec{u} - \vec{u}_p) + \frac{\vec{g}(\rho_p - \rho)}{\rho_p} \tag{5}$$

$$F_D = \frac{18\mu}{\rho_p d_p^2}\frac{C_D Re_p}{24} \tag{6}$$

where F_D is the drag force per unit particle mass, $\vec{u}$ is the fluid phase velocity, $\vec{u}_p$ is the particle velocity, ρ_p is the particle density, ρ is the fluid density, μ is the viscosity of the fluid, d_p is the particle diameter, and Re_p is the particle Reynolds number based on the relative velocity between particle and fluid. The term $\frac{\vec{g}(\rho_p-\rho)}{\rho_p}$ represents the buoyance force. From the hemodynamic principle, particles float along with the blood stream; hence, buoyancy force can be treated as neutral. The spherical drag law by Morsi and Alexander [29] is used to get the value of C_D.

$$C_D = \frac{24}{Re_p} \quad \text{for } Re_p < 1 \tag{7}$$

$$C_D = \frac{24}{Re_p}\left(1 + 0.015 Re_p^{0.687}\right) \quad \text{for } 1 < Re_p < 400 \tag{8}$$

$$Re_p = \frac{\rho d_p |\vec{u}_p - \vec{u}|}{\mu} \tag{9}$$

The trajectory equations of the particle are solved by stepwise integration over discrete time steps. Integration of time in Eq. (4) yields the velocity of the particle at each point along the trajectory. The differential equations are solved using Euler implicit discretization schemes.

2.4 Significance of Womersley Number in the Flow Field

The relationship between arterial size and pulse frequencies of hemodynamic natures expressed using non-dimensional number 'α' (Womersley number) [30] and is expressed as ($\alpha = R\sqrt{\omega/\upsilon}$), where R is the tube (artery) radius, ω is the angular frequency, and υ is the kinematic viscosity of the blood.

Physiological state of the human body is directly correlated with the Womersley number. A variation in the heart beat reflects in the pulse frequency of the blood flow. Change in pulse frequency will transform the laminar flow to a

weak turbulence flow [31]. Certain combination of pulse flow input and geometries (narrowed/complex) will generate vortices/helical flows in the flow field which may accelerate/decelerate the accumulation of new cells on to the arterial wall [14,26]

2.5 Significance of Helical Flow Field

Several studies have reported the presence of swirl flow in the human circulatory system [12,32,33]. During physiological states, certain combination of pulsatile flow through the non-planarity of arterial wall induce swirl/helical flow pattern in the vessel. Investigation of their study shows that swirl flow suppresses the localization of LDL and it accelerates mass transport in the lumen vessel. Due to spiral effect, early breakout of transitional to turbulence [7,34–37] may improve self-cleaning and rapid washout of flowing blood inside the blood vessel. Hence, helicity sign is a useful indicator of the rotational direction and/or intensity of the swirling fluid. Helical flow structure in the flow field has been analysed with swirl flow strength, and relative rotational direction is obtained by expressions derived from Gallo et al. [38].

$$h_1 = \frac{1}{TV}\int_T \int_V H \, \mathrm{d}v \, \mathrm{d}t \tag{10}$$

$$h_2 = \frac{1}{TV}\int_T \int_V |H| \, \mathrm{d}v \, \mathrm{d}t \tag{11}$$

$$h_3 = \frac{h_1}{h_2} \tag{12}$$

where T is the cardiac pulse cycle, V is the volume of fluid in domain, H is the swirl flow or helicity, and it can be expressed as $H = u.\omega$, where U is the velocity and ω is the vorticity of the fluid. To define the bulk flow parameter integration is carried out over time (T) and volume (V). The term h_1 is helical intensity, which is integral measure of helical flow accounting for helicity sign changes. h_1 equals '0' when there is no helical flow in the domain or it may have reflectional symmetric counter rotating helical structures. The parameter h_2 defines total amount of helical flow in the fluid domain, irrespective of direction. The term h_3 is a non-dimensional quantity ranging between -1 to $+1$. The h_3 value equals -1 $(+1)$ only when left-handed (right-handed) helical flow structures are present in the domain and it equals zero in case of reflectional symmetry or no helical structures in the flow field.

2.6 Grid Independence Study

The results of the numerical simulations must be independent of the number of grids used for the simulations. The grid independency study is also helpful to arrive at an optimum number of grids and to reduce computational time without compromising the accuracy of the solution. Hence, simulations are carried out for different number of grid elements keeping the same boundary conditions and the results are compared. The radial distribution of axial velocity profile has been plotted at $2D$ distance before the throat region of symmetric stenosis. The finest grid consisted of 0.93 million elements, and this has been taken as the reference grid to which results from other grids are compared. The coarse grid with 0.31 and 0.56 million elements is deviating far away from the finest grid. On the contrary, grids with 0.8 and 0.75 million elements show close match with the finest grid (Fig. 3). Hence, further numerical simulations are carried out on grid with 0.75 million elements due to the better accuracy and smaller computational time (10% lower than the convergence time of the finest grid). Similar procedure is adopted for the asymmetric model also, and optimum number of grid elements is identified to be 0.9 million.

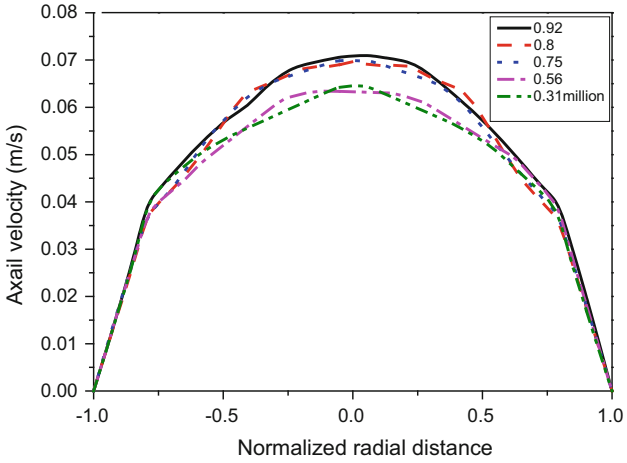

Fig. 3 Velocity profile at $-2D$ axial location for various grid elements

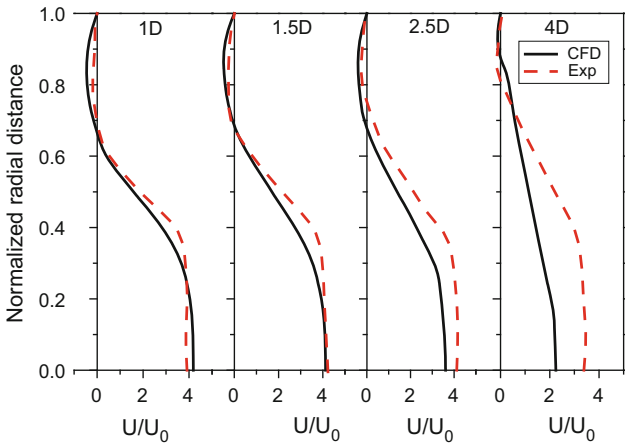

Fig. 4 Comparison of normalized velocity profile (U/U_0) at different axial locations with respect to normalized radial distance (r/R) at peak time step (T_2) in the post-stenosis region

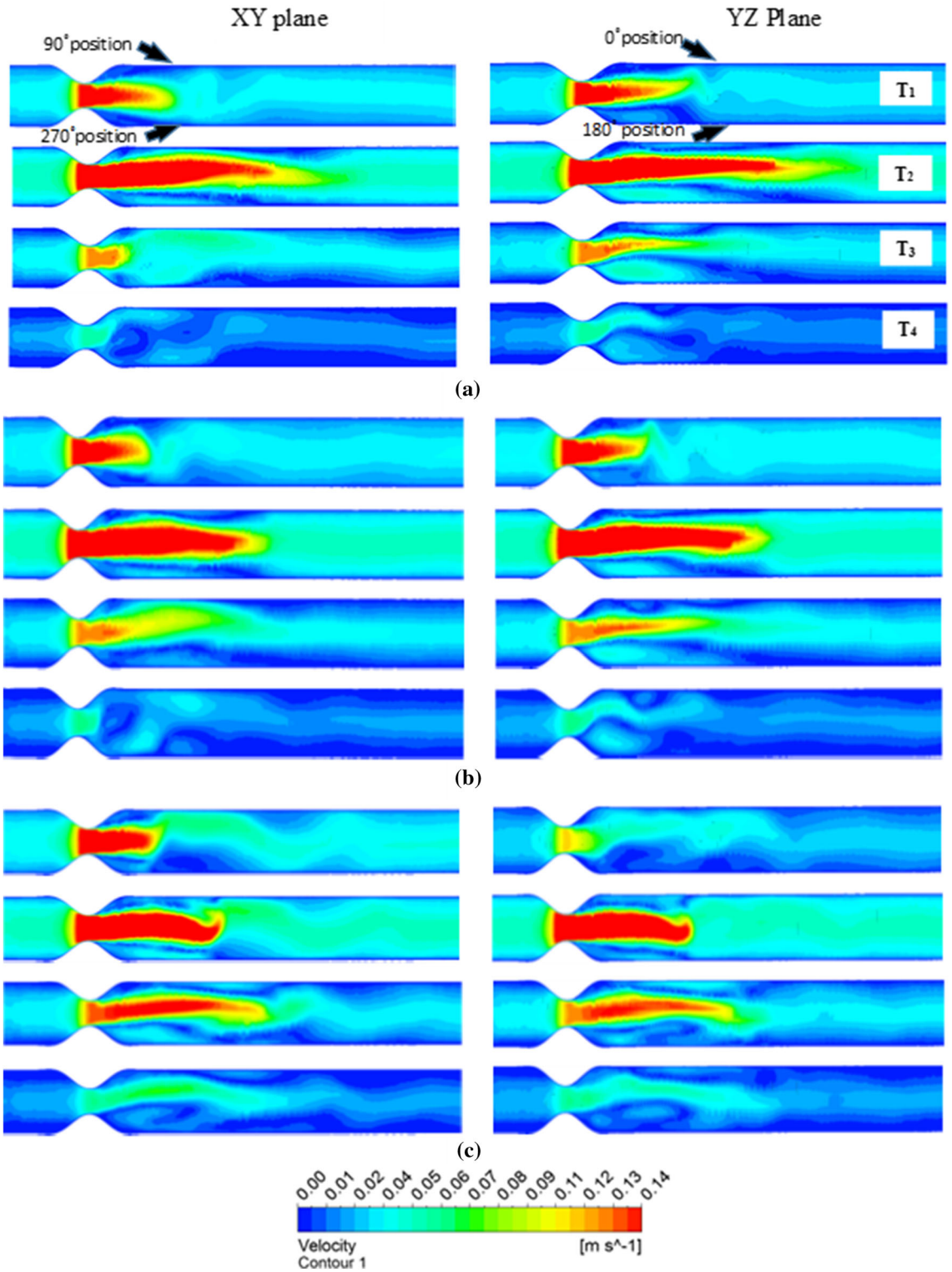

Fig. 5 Velocity contours for symmetric stenosis model **a** $\alpha = 7.5$. **b** $\alpha = 9$. **c** $\alpha = 12$

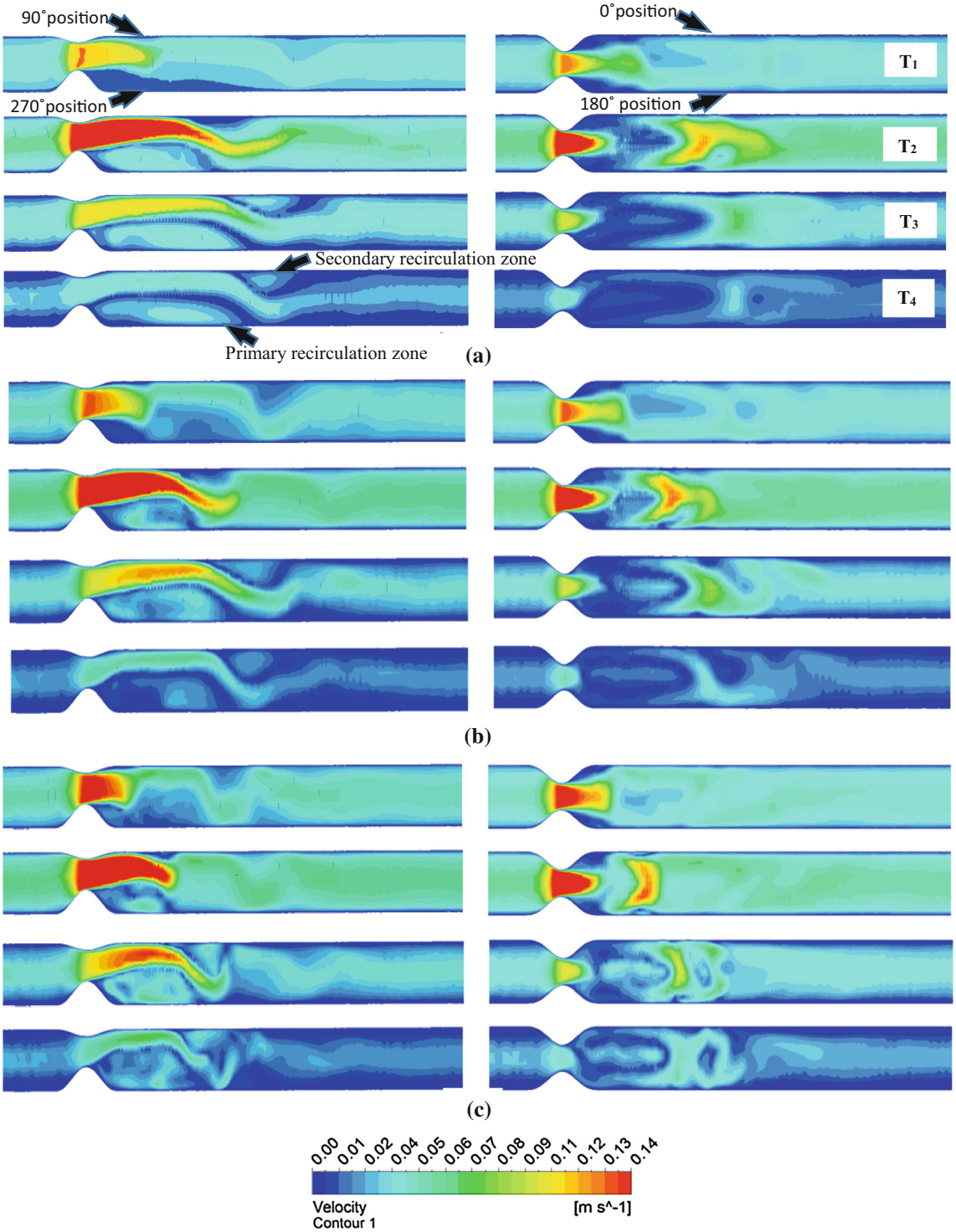

Fig. 6 Velocity contours for asymmetric stenosis model **a** $\alpha = 7.5$. **b** $\alpha = 9$. **c** $\alpha = 12$

2.7 Validation of the Numerical Methodology

In the numerical simulations of pulsatile flow through an idealized stenotic long tube, accurate results can be obtained only if the solution method is too appropriate. The causes of errors rises during discretizing and converging of Navier–Stokes governing equations. Hence, validation is an essential step in numerical simulations. In the present study, numerical results are validated with experimental results of Ahmed and Giddens [16] for the symmetric stenosed model under pulsatile flow. Comparisons are made for the radial variation of normalized axial velocity profile (U/U_0) at different axial

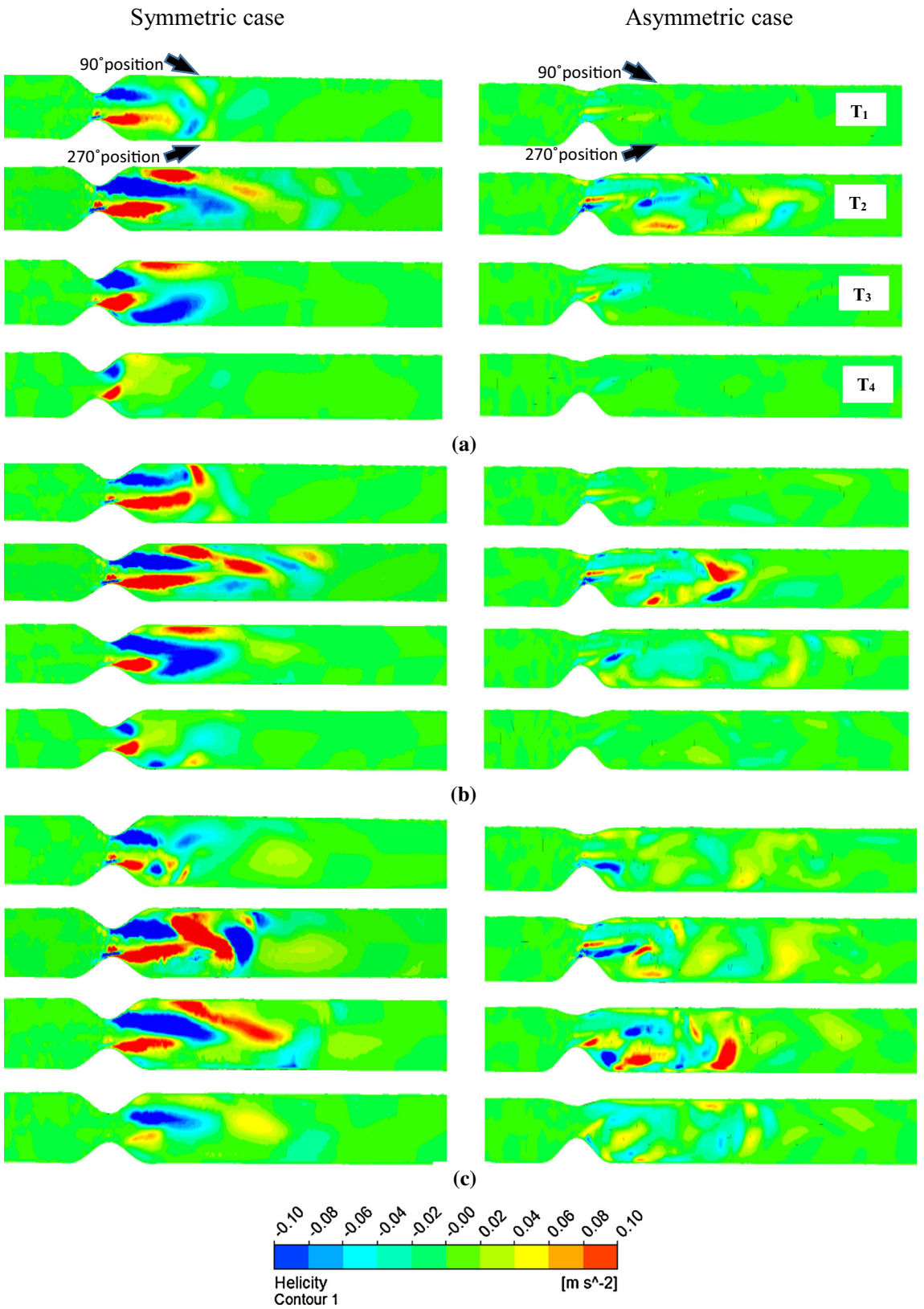

Fig. 7 Distributed Helicity contours in the asymmetric stenosis at different time instance of the pulse flow for **a** α = 7.5. **b** α = 9. **c** α =12

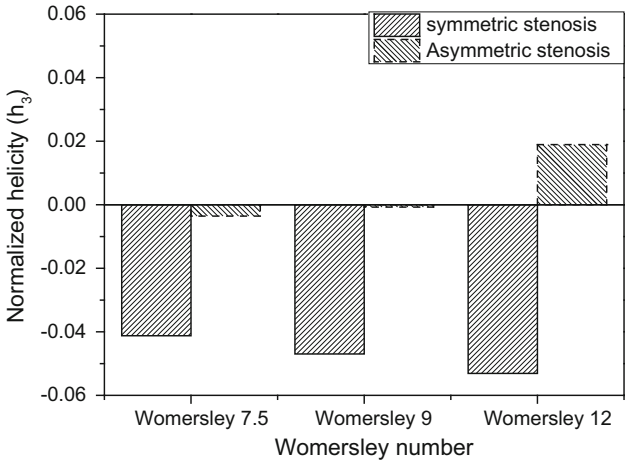

Fig. 8 Comparison of normalized helicity value for symmetric and asymmetric stenosis models at different Womersley numbers

locations, (viz. $1D$, $1.5D$, $2.5D$ and $4D$ distance) downstream to the minimum cross-sectional area (throat region) of stenosis. The results are plotted during peak cardiac time step (T_2) and shown in Fig. 4. The present computational results match both quantitatively and qualitatively with the experimental results quite well. Beyond $4D$ distance, computational results are under-predicted in comparison with the experimental values which has been also reported and justified previously by Ryval et al. [39] and Tan et al. [40].

3 Results and Discussion

3.1 Effect of Womersley Number on the Hemodynamics

As mentioned earlier, simulations are carried out at three different Womersley numbers (α) representing different pathological condition of a diseased human artery. To reveal the three-dimensional flow pattern, in the post-stenotic region, velocity contours are plotted at two orthogonal planes (0°–180° and 90°–270° planes). The evolution and development of the recirculation zones are monitored during the accelerating (T_1), peak (T_2), decelerating (T_3) and base points (T_4) of the pulse flow.

Figure 5 represents the velocity pattern for symmetrically stenosed model. A well-known jet type flow can be observed at the stenosis throat with thin shear layer that separates the

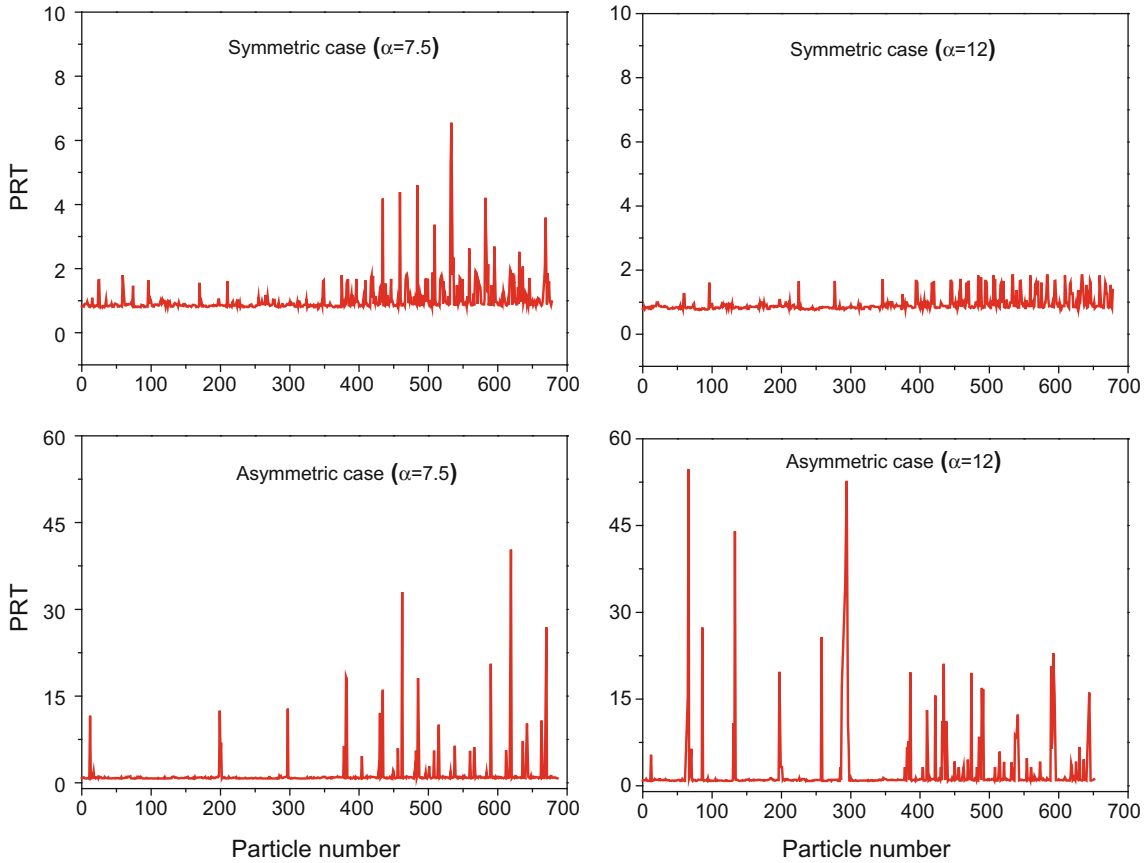

Fig. 9 Comparison of particle residence time (PRT) of 680 particles which are uniformly released from the inlet

Table 1 Mean particle residence time at different Womersley numbers (α)

Stenosis	Womersley number (α)	Mean PRT ($-2D$ to $6D$)
Symmetric case	7.5	1.025347
	12	0.938191
Asymmetric case	7.5	1.410647
	12	2.175722

recirculation zone at the periphery. The length of the jet region varies in accordance with the inlet flow profile. At higher Womersley number, the symmetric nature of jet flow lost and recirculation zones started losing. As a result, recirculation region on one side get thicker and pushes jet to the opposite wall. This results in a swaying movement of the jet region. It is to be noted that, with increase in Womersley number, length of the jet region diminishes with growing instabilities. At peak time step, the length of recirculation zone becomes smaller and point of reattachment shifts closer to the stenosis region.

For the asymmetric stenosis model also, the swaying motion of the jet region and the flow disturbances increase with Womersley number (Fig. 6). However, symmetric nature of the velocity profile no longer exists in the two selected orthogonal planes. In the 90°–270° plane (where the asymmetry is visible), the jet region bends towards the point of primary recirculation zone. Accordingly, opposite to the point of reattachment, a secondary recirculation zone develops. Long et al. [41] observed ring-shaped vortex structure at six diameter distal to the stenosis, which is formed by combination of primary and secondary vortices. In the present investigation also, this phenomenon is observed at lower Womersley number. However, at higher Womersley number an additional tertiary vortex is formed due to the higher instabilities and swaying movement of the jet region.

A better insight into the blood flow behaviour can be obtained by looking at the helicity contours. Helicity defines projection of a spin vector and represents the alignment of vorticity vectors in the fluid stream. Helicity is important at a fundamental level in relation to flow kinematics, and it states topological interpretation in relation to the linkages of vortex lines of the flow. If the spin vectors points in the same direction as the momentum vector, then the helicity is positive and if it is in opposite directions, then the helicity is negative. Helicity contours changes its sign across a separation or reattachment line [42].

Figure 7 shows the comparison of helicity plots for symmetric and asymmetric stenosis models. Proximal to the symmetric stenosis, strong helical structures but with opposite sign are seen to emerge from the upper and lower walls. Symmetric stenosis exhibits stronger linked vortices in comparison with the asymmetric case. Asymmetric stenosis model exhibits less helical flow structure than the symmetric stenosis model. Stretching of vortices and strong velocity fluctuations (weaker velocity zones) in the post-stenotic regions are the main causes for the distribution of weak helicity contours in the flow filed [43]. In other words, the vortical structures or the flow disturbances are not getting transported to the downstream side of the flow. This indicates that the probability of the atherogenic particles settling down at the post-stenotic region is much higher with increasing asymmetry of the stenosis.

The symmetric stenosis induces more helicity in the flow structure, due to more spinning nature flow, and hence, there will not be any chances of occlusion of new cells on the arterial wall. If the flow carries multiple linked vortices with high velocities, then it washes out the atherogenic particles along the arterial passage [7,38,44] demonstrating that the increased swirling flow can wash away atherogenic particles, thus suppressing the further development of plaque. The magnitude of helicity responds positively to the increase in the Womersley number. In the present investigations, the Womersley number is varied by increasing the pulse rate. Hence, an enhanced pulse rate during exercise or workout may increase the helical nature of the flow which washes out the atherogenic particles and minimizes the chances of plaque progression distal to stenosis. For the asymmetric stenosis model, strong helicity contours are absent; instead, the presence of low wake regions in the post-stenosis region provokes particles to settle on the wall. The linking of the vortices and their transportation along the mean blood flow is not seen even at higher Womersley number. This enhances the mass transport in the arterial flow which increases the burden of further atherogeneses distal to the stenosis.

Figure 8 represents the h_3 value calculated over the entire computational domain for different Womersley numbers. The symmetric stenosis model exhibits helicity several times higher than the asymmetric model. As a result, the relative residence time (the time of residence the molecules spent at endothelium) for the symmetric models is smaller than for the asymmetric stenosis model. With increase in the Womersley number, the normalized helicity increases steadily for symmetric stenosis, whereas the reverse holds true for asymmetric stenosis.

3.2 Analysis of the Discrete Phase

At the inlet of the computational domain, particles are distributed uniformly with a velocity that matches with the continuous phase and allowed to mix up with the transient pulsatile flow. The time required for the particles to travel from $-2D$ distance proximal to the stenosis to $6D$ distance distal to the stenosis location are calculated to get the particle

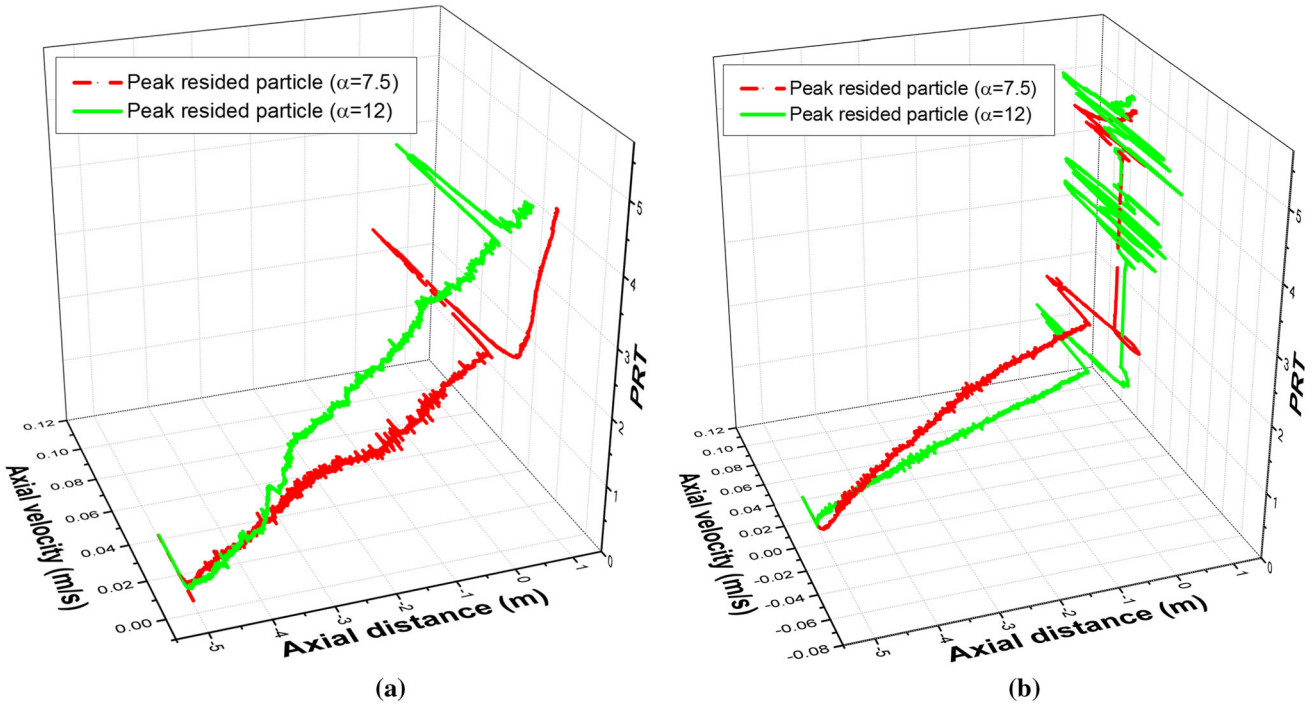

Fig. 10 Behaviour of peak resided particles inside the computational domain at different Womersley numbers

residence time (PRT). The PRT is defined as follows [14].

$$\mathrm{PRT} = \frac{T_{\mathrm{Trans}}}{T_{\mathrm{Steady}}} \tag{13}$$

where T_{Trans} is the time spend by the particle in the selected domain during transient simulation and T_{steady} is time spent by the particle in the selected domain during steady-state condition (i.e. at mean Reynolds number flow). As the computational effort involved in the discreet-phase modelling is too high, simulations are carried out only for the two extreme Womersley numbers (viz. 7.5 and 12). A total of 680 particles have been introduced at inlet, and their PRT analysis is shown in Fig. 9.

The analysis reveals that PRT of asymmetrical model is one order higher than the symmetric case. As there are multiple recirculation zones in the post-stenotic region of an asymmetric stenosis model, particles undergo looping and need longer time to escape from it. The mean particle residence time is shown in Table 1. The average residence time (mean PRT) for the symmetric stenosis model decreases with the Womersley number which can be attributed to the increased helicity in the symmetric stenosis model. On the other hand, the mean PRT value increases with the Womersley number for asymmetric stenosis model. This contradicting behaviour of asymmetric model is due to the presence of large localized recirculation zones. Unlike the symmetric model, the vortices formed in the post-stenotic regions are not getting carried away in the asymmetric model. The axis of the spinning vortices need not necessarily lie in the mean flow direction, and hence, there may not be a large value for helicity even though there are high flow disturbances and swirling strength for asymmetric stenosis model.

Plotting the trajectories of all the seeded particles in a single graph makes it cumbersome. Instead, the behaviour of peak resided particle inside the computational domain is shown in Fig. 10. The particles velocity and residence time are plotted against axial location. An axial distance zero refers to the minimum cross-sectional area (throat) of the stenosis. The axial velocities of the particles are almost similar for symmetric and asymmetric models up to the stenosis throat, beyond that significant differences are spotted in their behaviour. The particle trajectories of peak resided particle in a three-dimensional space are shown in Fig. 11. The erratic behaviour of the particles in the asymmetric model can be observed from this, especially at higher Womersley number. The effect of weaker flow regions near the wall enhances the PRT in the post-stenotic region which triggers further occlusion/plaque build-up [45,46]. This suggests that checking the extent of asymmetry in a diseased artery may be useful as the patient with higher eccentricity in stenosis may expect a faster progression of atherosclerosis.

3.3 Wall Shear Stress Distribution

Flow separation zones break into two parts in the post-stenotic region during systolic deceleration time instance

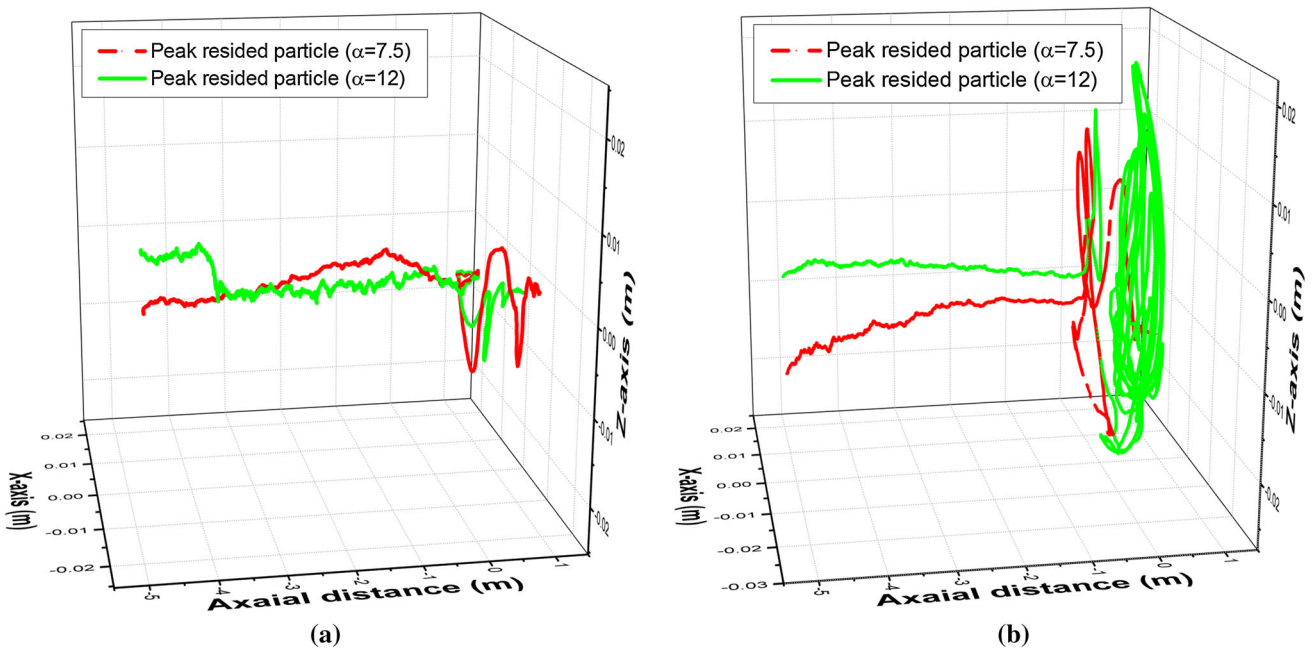

Fig. 11 Particle trajectories of the peak resided particle at different Womersley numbers

[41], and the flow disturbances are also high during this time instance. Hence, it is worth to analyse wall shear stress (WSS) distribution during deceleration time step (T_3). The asymmetry of the stenosis lies on the 90°–270° plane, and the primary and secondary recirculation zones are more visible in this plane. Hence, the wall shear stress variations are noted on two polylines, which are running along the 90° and 270° angular position of the arterial wall from $-2D$ distance to $14D$ distance. An increase in frequency in the pulse provokes more oscillations in the flow filed which are reflected in the WSS distribution also in the form of ups and downs. The WSS values are normalized with their corresponding spatial average value and shown along the axial directions in Fig. 12.

The normalized value of WSS for an asymmetric stenosis model is lower than for the symmetric one in one side of the arterial wall (90°). The WSS peaks at the stenosis throat region (correspond to zero axial location) come to a steady value at an axial location of 0.5 m. Majority of the oscillations in the WSS values are focused close to the stenosis region for the symmetric model, whereas in the case of an asymmetric stenosis model, the undulations are more severe slightly away from the stenosis region, more specifically at regions between 0.15–0.35 m. Yakhot et al. [47] also noticed oscillations in the WSS values are triggered by the presence of secondary vortices which are seen only in an asymmetric stenosed artery. The WSS value rises at the point where the primary vortex reattaches to the wall. In other words, blood flow is constricted at the reattachment point due to the blockage created by the secondary vortices. This causes a rise in the WSS at this location, and it become stronger at higher Womersley number.

4 Conclusions

The present computational study investigates the effect of pulse flow rate on the hemodynamics and atherogenic particles behaviour through discrete-phase modelling. The studies are carried out in an idealized symmetric and asymmetric stenosis models, and the following major conclusions are derived.

Helicity in the post-stenotic region can be considered as an indicator for the progression of the atherosclerosis, as it directly influences the particle residence time (PRT) at that region. The asymmetric stenosis model exhibits less helical flow structure than the symmetric stenosis model. The vortical structures or the flow disturbances are not getting transported to the downstream side of the flow, which enhances the mass transport in the arterial flow and triggers further occlusion/plaque build-up at the post-stenotic region. Consequently, the mean PRT values of the atherogenic particles are one order higher than the symmetric stenosis model. On the other hand, symmetric stenosis induces more helicity in the flow structure and hence the chances of occlusion of new cells on the arterial wall are minimal. The average residence time (mean PRT) for the symmetric stenosis model decreases with the Womersley number due to the increased helicity. Contrary to this, the mean PRT value increases with the Womersley number for asymmetric stenosis model.

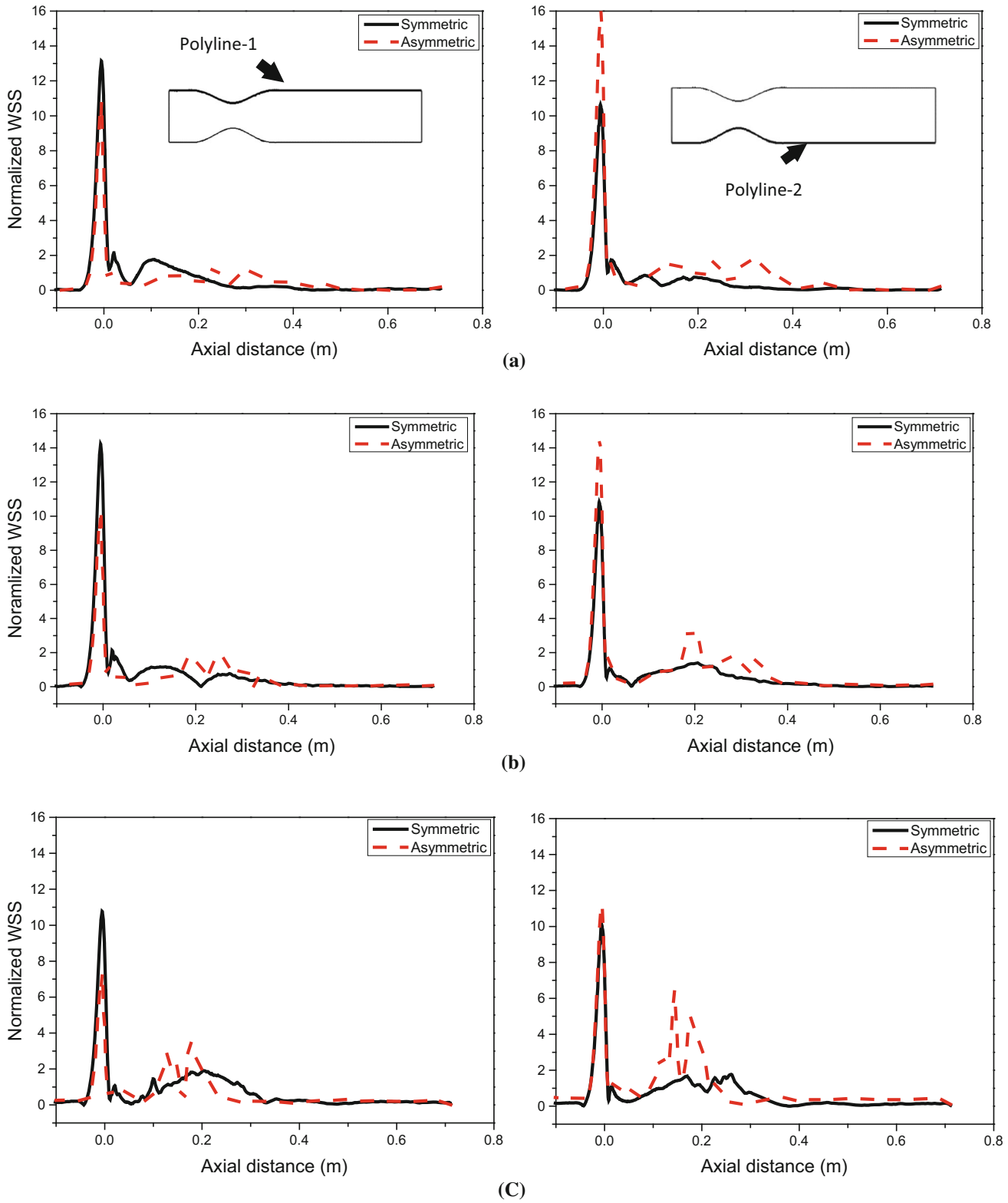

Fig. 12 Spatial variation of wall shear stress at different Womersley numbers **a** $\alpha = 7.5$. **b** $\alpha = 9$ and **c** $\alpha = 12$

More number of localized vortices are found to occur in the asymmetric stenosed model. Unlike the symmetric model, the vortices formed in the post-stenotic regions are not getting transported in the asymmetric model. The formation of secondary vortices in asymmetric model leads to severe undulations in the WSS distribution distal to the stenosis throat region. The extent of asymmetry in a diseased artery may be considered as a useful parameter in understanding the rate of progression of atherosclerosis.

References

1. Stroud, J.; Berger, S.; Saloner, D.: Numerical analysis of flow through a severely stenotic carotid artery bifurcation. J. Biomech. Eng. **124**, 9–20 (2002)
2. Liu, B.: The influences of stenosis on the downstream flow pattern in curved arteries. Med. Eng. Phys. **29**, 868–76 (2007)
3. Pagiatakis, C.; Tardif, J.-C.; L'Allier, P.L.; Mongrain, R.: Effect of stenosis eccentricity on the functionality of coronary bifurcation lesions—a numerical study. Med. Biol. Eng. Comput. **55**, 2079–95 (2017)
4. Varghese, S.S.; Frankel, S.H.; Fischer, P.F.: Modeling transition to turbulence in eccentric stenotic flows. J. Biomech. Eng. **130**, 014503 (2008)
5. Dvinsky, A.; Ojha, M.: Simulation of three-dimensional pulsatile flow through an asymmetric stenosis. Med. Biol. Eng. Comput. **32**, 138–42 (1994)
6. Jabir, E.; Lal, S.A.: Numerical analysis of blood flow through an elliptic stenosis using large eddy simulation. Proc. Inst. Mech. Eng. Part H J. Eng. Med. **230**, 709–26 (2016)
7. Ha, H.; Choi, W.; Park, H.; Lee, S.J.: Effect of swirling blood flow on vortex formation at post-stenosis. Proc. Inst. Mech. Eng. Part H J. Eng. Med. **229**, 175–83 (2015)
8. Basavaraja, P.; Surendran, A.; Gupta, A.; Saba, L.; Laird, J.R.; Nicolaides, A.; et al.: Wall shear stress and oscillatory shear index distribution in carotid artery with varying degree of stenosis: a hemodynamic study. J. Mech. Med. Biol. **17**, 1750037 (2017)
9. Evegren, P.; Fuchs, L.; Revstedt, J.: Wall shear stress variations in a 90-degree bifurcation in 3d pulsating flows. Med. Eng. Phys. **32**, 189–202 (2010)
10. Chiastra, C.; Gallo, D.; Tasso, P.; Iannaccone, F.; Migliavacca, F.; Wentzel, J.J.; et al.: Healthy and diseased coronary bifurcation geometries influence near-wall and intravascular flow: a computational exploration of the hemodynamic risk. J. Biomech. **58**, 79–88 (2017)
11. Ku, D.N.; Giddens, D.P.; Zarins, C.K.; Glagov, S.: Pulsatile flow and atherosclerosis in the human carotid bifurcation. Positive correlation between plaque location and low oscillating shear stress. Arterioscler. Thromb. Vasc. Biol. **5**, 293–302 (1985)
12. Morbiducci, U.; Ponzini, R.; Rizzo, G.; Cadioli, M.; Esposito, A.; Montevecchi, F.M.; et al.: Mechanistic insight into the physiological relevance of helical blood flow in the human aorta: an in vivo study. Biomech. Model. Mechanobiol. **10**, 339–55 (2011)
13. Perktold, K.; Resch, M.; Peter, R.O.: Three-dimensional numerical analysis of pulsatile flow and wall shear stress in the carotid artery bifurcation. J. Biomech. **24**, 409–20 (1991)
14. Buchanan Jr., J.; Kleinstreuer, C.; Comer, J.: Rheological effects on pulsatile hemodynamics in a stenosed tube. Comput. Fluids **29**, 695–724 (2000)
15. Banerjee, M.K.; Ganguly, R.; Datta, A.: Effect of pulsatile flow waveform and womersley number on the flow in stenosed arterial geometry. ISRN Biomathematics 2012 (2012)
16. Ahmed, S.A.; Giddens, D.P.: Pulsatile poststenotic flow studies with laser doppler anemometry. J. Biomech. **17**, 695–705 (1984)
17. Tang, D.; Yang, C.; Kobayashi, S.; Zheng, J.; Vito, R.P.: Effect of stenosis asymmetry on blood flow and artery compression: a three-dimensional fluid-structure interaction model. Ann. Biomed. Eng. **31**, 1182–93 (2003)
18. Lee, S.-W.; Steinman, D.A.: On the relative importance of rheology for image-based cfd models of the carotid bifurcation. J. Biomech. Eng. **129**, 273–78 (2007)
19. Frattolin, J.; Zarandi, M.M.; Pagiatakis, C.; Bertrand, O.F.; Mongrain, R.: Numerical study of stenotic side branch hemodynamics in true bifurcation lesions. Comput. Biol. Med. **57**, 130–38 (2015)
20. Li, G.; Hu, R.; Gao, F.: Numerical simulation of coronary artery stenosis before and after stenting. J. Med. Biol. Eng. **35**, 528–34 (2015)
21. Tarbell, J.M.: Mass transport in arteries and the localization of atherosclerosis. Annu. Rev. Biomed. Eng. **5**, 79–118 (2003)
22. Ethier, C.R.: Computational modeling of mass transfer and links to atherosclerosis. Ann. Biomed. Eng. **30**, 461–71 (2002)
23. Zhang, Z.-G.; Zhang, X.-W.; Liu, Y.-X.: Effects of fluid recirculation on mass transfer from the arterial surface to flowing blood. Acta Mech. Sin. **28**, 904–10 (2012)
24. Lebanon, N.: Fluent 6.1 user's guide (2003)
25. Peterson, S.D.; Plesniak, M.W.: The influence of inlet velocity profile and secondary flow on pulsatile flow in a model artery with stenosis. J. Fluid Mech. **616**, 263–301 (2008)
26. Banks, J.; Bressloff, N.: Turbulence modeling in three-dimensional stenosed arterial bifurcations. J. Biomech. Eng. **129**, 40–50 (2007)
27. Mukherjee, D.; Padilla, J.; Shadden, S.C.: Numerical investigation of fluid-particle interactions for embolic stroke. Theor. Comput. Fluid Dyn. **30**, 23–39 (2016)
28. Zhang, Z.; Fan, Y.; Deng, X.: Oxygen transfer in human carotid artery bifurcation. Acta Mech. Sin. **23**, 305–09 (2007)
29. Morsi, S.; Alexander, A.: An investigation of particle trajectories in two-phase flow systems. J. Fluid Mech. **55**, 193–208 (1972)
30. Womersley, J.R.: Method for the calculation of velocity, rate of flow and viscous drag in arteries when the pressure gradient is known. J. Physiol. **127**, 553–63 (1955)
31. Ojha, M.; Cobbold, R.S.; Johnston, K.W.; Hummel, R.L.: Pulsatile flow through constricted tubes: an experimental investigation using photochromic tracer methods. J. Fluid Mech. **203**, 173–97 (1989)
32. Houston, J.G.; Gandy, S.J.; Sheppard, D.G.; Dick, J.B.; Belch, J.J.; Stonebridge, P.A.: Two-dimensional flow quantitative mri of aortic arch blood flow patterns: effect of age, sex, and presence of carotid atheromatous disease on prevalence of spiral blood flow. J. Magn. Reson. Imaging **18**, 169–74 (2003)
33. Stonebridge, P.; Brophy, C.: Spiral laminar flow in arteries? The Lancet **338**, 1360–61 (1991)
34. Ha, H.; Lee, S.-J.: Hemodynamic features and platelet aggregation in a stenosed microchannel. Microvasc. Res. **90**, 96–105 (2013)
35. Ha, H.; Lee, S.J.: Effect of pulsatile swirling flow on stenosed arterial blood flow. Med. Eng. Phys. **36**, 1106–14 (2014)
36. Gataulin, Y.A.; Zaitsev, D.K.; Smirnov, E.M.; Fedorova, E.A.; Yukhnev, A.D.: Weakly swirling flow in a model of blood vessel with stenosis: numerical and experimental study. St. Petersburg Polytechnical University. J. Phys. Math. **1**, 364-71 (2015)
37. Ha, H.; Hwang, D.; Choi, W.-R.; Baek, J.; Lee, S.J.: Fluid-dynamic optimal design of helical vascular graft for stenotic disturbed flow. PLoS ONE **9**, e111047 (2014)
38. Gallo, D.; Steinman, D.A.; Bijari, P.B.; Morbiducci, U.: Helical flow in carotid bifurcation as surrogate marker of exposure to disturbed shear. J. Biomech. **45**, 2398–404 (2012)
39. Ryval, J.; Straatman, A.; Steinman, D.: Two-equation turbulence modeling of pulsatile flow in a stenosed tube. J. Biomech. Eng. **126**, 625–35 (2004)

40. Tan, F.; Soloperto, G.; Bashford, S.; Wood, N.; Thom, S.; Hughes, A.; et al.: Analysis of flow disturbance in a stenosed carotid artery bifurcation using two-equation transitional and turbulence models. J. Biomech. Eng. **130**, 061008 (2008)
41. Long, Q.; Xu, X.; Ramnarine, K.; Hoskins, P.: Numerical investigation of physiologically realistic pulsatile flow through arterial stenosis. J. Biomech. **34**, 1229–42 (2001)
42. Moffatt, H.; Tsinober, A.: Helicity in laminar and turbulent flow. Annu. Rev. Fluid Mech. **24**, 281–312 (1992)
43. Hunt, J.; Hussain, F.: A note on velocity, vorticity and helicity of inviscid fluid elements. J. Fluid Mech. **229**, 569–87 (1991)
44. Zovatto, L.; Pedrizzetti, G.: Fluid flow in a helical vessel in presence of a stenosis. Meccanica **52**, 545–53 (2017)
45. Ma, P.; Li, X.; Ku, D.N.: Convective mass transfer at the carotid bifurcation. J. Biomech. **30**, 565–71 (1997)
46. Fatouraee, N.; Deng, X.; Champlain, A.; Guidoin, R.: Concentration polarization of low density lipoproteins (ldl) in the arterial system. Ann. N. Y. Acad. Sci. **858**, 137–46 (1998)
47. Yakhot, A.; Grinberg, L.; Nikitin, N.: Modeling rough stenoses by an immersed-boundary method. J. Biomech. **38**, 1115–27 (2005)